Real-time monitoring of temperature rises of energized transformer cores with distributed optical fiber sensors

Ping Lu, Michael P. Buric, Kevin Byerly, Seungryul Moon, Mst. Nazmunnahar, Satoru Simizu, Alex Leary, Byron Beddingfield, Chenhu Sun, Paul Zandhuis, Michael E. McHenry, and Paul R. Ohodnicki

***Abstract* -- Real-time temperature mapping that solves local overheating problems is important for obtaining an optimized thermal design for high-efficiency power transformers. Internal temperature monitoring of operating power transformers can also be leveraged for asset monitoring applications targeting at fault detection enabling condition-based maintenance. Transformers present a variety of challenging sensing environments such as high-levels of electromagnetic interference and limited space for conventional sensors to operate. Immersion of power transformers in insulation oils for thermal management during operation and the presence of relatively large and time varying electrical and occasional magnetic fields make sensing technologies requiring electrical wires or active power at sensing locations highly undesirable. In this work, we investigate thermal response of a standard telecom fiber instrumented on compact transformer cores by using an optical frequency-domain reflectometry scheme. Correlation between conventional temperature sensing methods and fiber-optic sensing results as well as trade-offs between spatial resolution and temperature measurement accuracy is discussed and spatially resolved real-time monitoring of temperatures in energized transformers is experimentally demonstrated.**

Index Terms--Optical fiber sensors, temperature sensors, Rayleigh scattering, optical frequency-domain reflectometry, transformer cores.

I. Introduction

TRANSFORMERS play an important role in the power transmission and distribution system [1]. High operating temperature conditions resulting from the associated core and winding losses within transformers limit transformer performance and lifetime [2]. An optimum thermal design can enable construction of more compact and efficient transformers by accurately measuring temperature profiles for various candidate designs, including potentially complex-shaped core layouts in a distributed and real-time fashion. In addition, real-time monitoring methods enable spatially resolved temperature monitoring at various locations on an energized magnetic core, paving the way for on-line monitoring of electrical assets that can identify early evidence of faults, enabling condition-based maintenance programs to be instituted before catastrophic failure is observed [3], [4]. Asset monitoring of large power transformers is an area of key importance due to high economic and social costs associated with bulky and expensive grid assets like large power transformers that are custom components with a limited domestic supply chain [5-7]. Demands for higher power densities, more modular solutions, and advanced functionality for power electronics converters are also increasing because of many emerging applications. The new applications include grid integration of distributed energy resources, electrification of military, aviation, aerospace, and automotive vehicles, and the development of modular and compact solid-state transformers [8].

To achieve an optimal combination of power density, functionality, and efficiency, a detailed understanding of the thermal profile is critical for successful thermal management. The thermal profile begins to play an important role and even dominates designs in some cases where the transformer components are being pushed to higher operational frequencies for maximized power densities. With the emergence of new wide-bandgap semiconductor switching devices, transformers and other inductive components are pushed to frequencies, power levels, and power densities not previously attainable [9]. Design via thermal numerical modelling and simulation can become an integral part of the power system design process as a less expensive solution than a purely experimental approach [10], [11]. Ultimately the potential of analytical models and/or finite-element-based analyses must be confirmed by actual measurements and comparisons. Direct temperature monitoring outside or inside the transformer can be obtained through

Ping Lu, Kevin Byerly, Seungryul Moon, and Paul Zandhuis are with AECOM and National Energy Technology Laboratory, Pittsburgh, PA 15236, USA (e-mail: Ping.Lu@netl.doe.gov; Kevin.Byerly@netl.doe.gov; Seungryul.Moon@netl.doe.gov; Paul.Zandhuis@netl.doe.gov).

Michael P. Buric is with National Energy Technology Laboratory, Morgantown, WV 26505, USA (e-mail: Michael.Buric@netl.doe.gov)

Mst. Nazmunnahar, Satoru Simizu, and Michael E. McHenry are with Materials Science & Engineering Department, Carnegie Mellon University, Pittsburgh, PA 15213, USA (e-mail: mnazmunn@andrew.cmu.edu; simizu@andrew.cmu.edu; mm7g@andrew.cmu.edu).

Alex Leary is with the NASA Glenn Research Center, Cleveland, OH 44135, USA (e-mail: alex.m.leary@nasa.gov).

Byron Beddingfield is with the Department of Electrical and Computer Engineering, North Carolina State University, Raleigh, NC 27606, USA (e-mail: rbbeddin@ncsu.edu).

Chenhu Sun and Paul R. Ohodnicki are with National Energy Technology Laboratory, Pittsburgh, PA 15236, USA and Paul R. Ohodnicki is also with Materials Science & Engineering Department, Carnegie Mellon University (e-mail: Chenhu.Sun@netl.doe.gov; Paul.Ohodnicki@netl.doe.gov).

several methods. Conventional electrical signal demodulation methods with thermocouples and other similar components are susceptible to electromagnetic interference (EMI). Stray electromagnetic fields emanating from high-power, low-frequency transformers and high-frequency fields from power electronics converter isolation transformers subject electrically conductive temperature sensors to high rates of flux change. It induces eddy currents on the sensors leading to measurement noise and potential sensor heating. The infrared temperature measurement method is mainly used for occasional hot-spot inspection rather than online detection but requires direct optical access to the surface being measured. The process of integrating optical fiber sensors in harsh power-systems environments has attracted great interest during recent decades because of unique advantages such as immunity to EMI, high sensitivity, fast response, and the potential of monitoring multiple parameters simultaneously. Optical fiber probes for the measurement of hot-spot temperatures in transformers have been introduced over the last two decades [12-18].

The first ferromagnetic amorphous metallic alloys were produced by splat quenching [19] and the first ferromagnetic alloy produced as an amorphous magnetic ribbon (AMR) was $Fe_{80}P_{13}C_7$ [20], [21]. The effects of metalloids on glass forming ability in Fe led to commercialization of metallic glasses for magnetic applications, the first produced by Allied Signal in 1973 [22]. The Fe-B system was developed for AMR [23], [24] and soon followed by Fe-B-Si [25], [26] and Fe-B-Si-C [27], [28]. These alloys exhibited significantly lower losses than Si-steels and improved efficiency led to further development. In 1978 the first amorphous alloy transformer core was introduced and a pilot continuous casting line was built in 1979. In 1982 Allied Signal installed the first amorphous transformer cores in the U.S. and in 1989 began production of transformer core alloys. Honeywell's Metglas Division was purchased in 2003 by Hitachi Metals. Hitachi Metals developed the first nanocrystalline soft magnetic material, named Finemet [29]. Recent developments considered as derivative from amorphous metals can be enumerated in terms of structural distinctions [30]. Multiphase metal/amorphous nanocomposite (MANC) materials are produced by subsequent controlled crystallization of a multicomponent amorphous precursor to yield a nanocrystalline phase embedded in an amorphous matrix [31]. Both provide functionality to the MANC [32].

In this study, a high-sensitivity and high spatial resolution fiber-based optical frequency-domain reflectometry (OFDR) system is employed to measure distributed temperature rises in MANC cores in operation. The proposed method by using the fiber itself as a sensing medium provides excellent opportunity for distributed temperature monitoring of power transformers by allowing measurements to be taken along the entire length of the fiber rather than at discrete points. OFDR provides spatial resolution ranging from a few microns for a fiber that is a few meters long, to a few centimeters for a several-kilometer long fiber [33-37]. It fills the gap in the measurement resolution and range between optical time-domain reflectometry [38] and optical low-coherence reflectometry [39], so that it becomes very attractive for practical temperature and strain monitoring applications in structural health monitoring. In this application, we see a similar fit between system-measurement resolution and real-world requirements. The experiment will detail effectiveness of measurements made using an OFDR system focusing on fiber-installation to minimize temperature/strain cross-sensitivity effects when the transformer is in operation. This work provides a new approach to achieving distributed real-time temperature sensing that can be further improved by adopting new optical fiber structures or data processing schemes.

II. Experimental Details

Rayleigh scattering in optical fiber is caused by random fluctuations in the refractive index profile along the fiber length induced during the fiber fabrication process, which represents permanent structural strain or impurity properties in the fiber. Changes in the local characteristics of the single-mode sensing fiber due to surrounding temperature changes cause changes in the Rayleigh backscatter spectrum. A cross-correlation between the Rayleigh backscatter spectra of the reference and measurement profiles leads to a temperature-dependent spectral shift. Distributed temperature measurement along the entire sensing fiber length can be achieved by calibrating these spectral shifts to known temperatures via an initial calibration. An OFDR based distributed fiber optic temperature sensing system is characterized by the spatial resolution and temperature accuracy. It is highly required to achieve high accuracy temperature measurement with fine spatial resolution.

The transformer excitation conditions are varied while measuring core temperature using a commercial OFDR system (OBR4600, Luna). Optical fiber sensors for analyzing dissolved gases in a wide range of oil filled power assets have been intensively studied, as indicated in Ref [5]. The sensing fiber used in this study is a type of standard telecommunication grade fiber well-known for its ruggedized product portfolio necessary to endure environmental and mechanical rigors found in oil and gas, transportation, and energy infrastructures. Figure 1 illustrates a schematic diagram of the configuration of the OFDR based sensing system including the layout of the sensing fiber instrumented on the transformer core. The sensing fiber is a telecommunication single-mode fiber (SMF28, Corning) fusion spliced with a single-mode fiber patch cable terminated with an APC connector. The termination end of the sensing fiber is coiled into a ring of a very small diameter to minimize Fresnel reflections from the end-face of the fiber. The sensing fiber is mounted on the four faces of the racetrack-shaped transformer core (front, inside, back left-leg, back right-leg, and outside) as well as inner/outer loops. It should be indicated that the sensing fiber with a diameter of 250μm can fit millimeter-order gaps between windings. Thus the mounted sensing fiber can essentially cover every measuring points along the length of the windings. Mounting is accomplished by coating the fiber with thermally conductive paste and sticking the paste-coated fiber directly to the core surface. This method is used to minimize pre-strain in the fiber, while maximizing thermal

conductivity between the core and fiber. Large loops of fiber are left to dangle in free air when traversing between two measurement surfaces. It permits clear identification of the surface location in the measured temperature profile, as well as ensuring that bending losses do not adversely affect the measurement region. It is noted that no extra glass fiber is needed to assist the high mechanical strength and reliability sensing fiber in passing safely through the tank wall to different areas inside a power transformer.

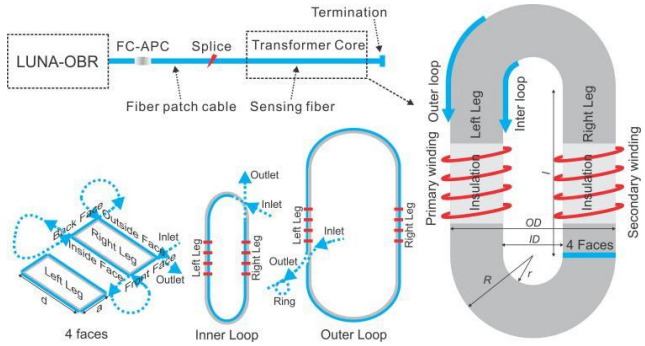

Fig. 1. Schematic diagram of the OFDR based sensing system including the layout of the sensing fiber instrumented on the transformer core.

To demonstrate the application of OFDR for continuous on-line temperature monitoring in power transformers, two single-phase transformer cores are operated and measured: a Hitachi FT-3TL core of composition $Fe_{73.5}Si_{15.5}B_{7.0}Nb_{3.0}Cu_{1.0}$ [40] and a $Fe_{72.9}Si_{16.2}B_{6.9}Nb_{3.0}Cu_{1.0}$ MANC core [41]. The dimensions of two magnetic cores are shown in Fig. 2. Planar flow casting is used for ribbon production in transformer fabrication. The core is left uncut to lessen the impact of fringing flux and other imperfections. The constructed transformer is subjected to an open secondary test by using a custom-developed H-bridge based bipolar excitation circuit. Transformer core losses and thermal field distribution are evaluated by exciting the core with waveforms on the primary winding that are relevant for deployment in medium-frequency power electronics and power conversion applications. The custom excitation circuit employs SiC-based semiconductor JFET devices and is rated for excitation voltages approaching 800V with a DC power supply rated for up to 15 kW.

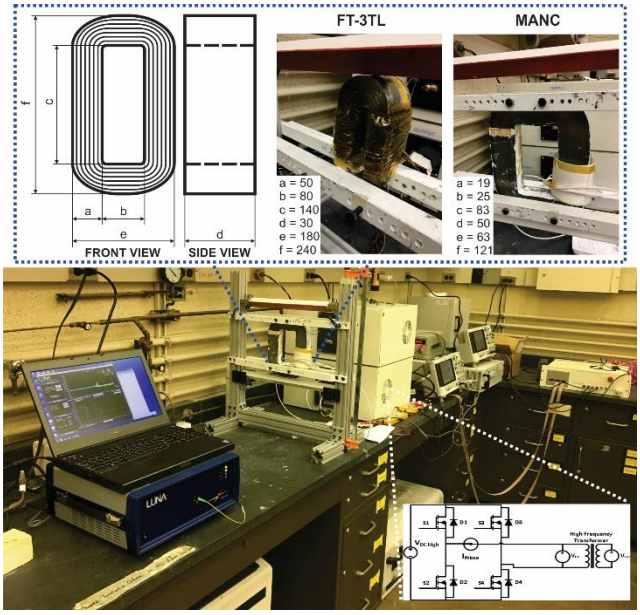

Fig. 2. Experimental setup for distributed temperature monitoring of the compact transformers.

The experimental arrangement for fiber-based distributed temperature monitoring of a single-phase transformer is shown in Fig. 2. Each core section has a 3 mm OD nylon-wrapped Type 2 Litz-wire 4-turn winding, insulated with Nomex® and Kapton tape. The core is attached to an extruded aluminum and fiberglass frame to enable testing with minimal impacts from strain and stray field induced losses. The primary winding and secondary winding are placed on adjacent sections around the core under test. The primary winding is excited with a square wave shaped waveform and a fixed frequency of 50 kHz with duty cycle of 50%. A DC power supply generates the input voltage. The current on the primary winding is measured by using an AC/DC current probe and the voltage on the open secondary winding is measured by using a differential voltage probe with attenuation ratio of 1:20. The thermal field distributions induced by the core losses are measured under natural convection free air cooling.

III. Results and Discussion

After calibrating the spectral shift in the fiber to known temperatures, detailed measurement of core-heating is produced for both FT-3TL and MANC cores. Finite element method (FEM) analysis, standard IR-based thermal imaging measurements, energy loss measurements, and fiber-optic sensing results are then compared and discussed. A trade-off between spatial resolution and temperature sensing accuracy is theoretically analyzed and then applied to actual test results where different levels of temperature-perturbation occurs. The proposed method can easily be extended to cover situations in which both high-accuracy and high-spatial resolution thermal surveillance are required in the same application. This offers the potential for unprecedented optimization of magnetic core designs for power transformer applications as well as a novel approach to power transformer asset real-time monitoring.

A. Type FT-3TL Core

To test this core, the excitation winding is connected to a square-wave voltage generator to induce triangular current waveforms. The applied square voltage waveform to an inductive load resulting in triangular current waveforms is often encountered in power electronics applications, and such waveforms cause energy losses in the transformer cores. The transformer generates energy loss that is converted to heat once the transformer is in operation as a result of various sources of core loss including hysteresis, eddy current, anomalous eddy current, and primary or secondary winding resistance. The current in the primary winding and the induced voltage on the secondary winding are utilized to measure the energy loss in the core based on the hysteresis loop characteristic measurement technique [42]. The amplitude of the square-wave excitation voltage was increased to 100V, 175V, and 250V for 20 minutes each, as shown in Fig. 3.

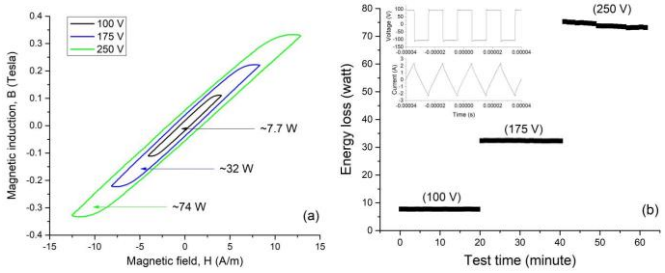

Fig. 3. (a) B-H curves under different excitation voltages; (b) Calculated core loss under different excitation voltages. Inset shows the excitation voltage and current on the primary winding.

To compare the OFDR-based distributed fiber optic temperature sensing method to the infrared thermography technique, a thermal imaging camera is used which has a spectral band of 8μm to 14μm and exhibits thermal accuracy of 2°C. It has a spatial resolution of 2.2 mrad for a field of view of 20° x 15° with a microbolometer consisting of a focal plane array of 160x120 pixels in the magnification shown. The images registered by the thermal camera are illustrated in Fig. 4. Initially, the transformer has the hottest spot near the inner core surface, as expected for open secondary excitation measurements due to the difference in local flux concentration at the inner radius of a toroid as compared to the outer radius.

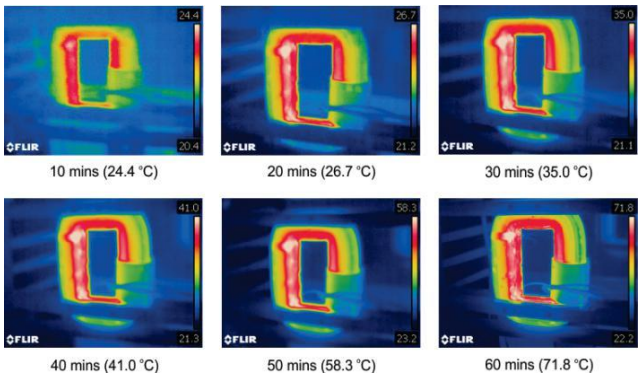

Fig. 4. Thermal view of the transformer core recorded at different time.

Coupled electromagnetic-thermal modeling of transformer core-winding is achieved by Finite Element Analysis software COMSOL Multiphysics [43, 44]. The source of thermal fields is assumed to be the heat converted from core losses due to core excitation flux which are characterized by the Steinmetz equation and Joule losses in windings. The spatial distribution of the magnetic and electric fields as well as the flux leakage to the surrounding air medium is computed considering the effect of a nonlinear B-H curve in the core. The windings are assumed to have a uniform volumetric heating source related to the current density and the resistivity, provided that effects which produce spatially varying losses within the windings (such as proximity losses) are negligible. Figure 5(a) shows a surface plot of the magnetic flux density normal distribution and the contour plot of the magnetic vector potential in the core at t = 0.01ms. The losses varying with the local peak flux density within the excited transformer core in a short observation period dissipate in the form of heat and cause the temperature rise of the transformer. The steady state heat conduction equation governs the heat flow inside the core and Newton's law of cooling holds true for describing the convective heat transfer at the interface between the core and ambient air. Figure 5(b) illustrates that the core with winding-resistance induced heating has MAX/MIN temperature of 388K/384K while the core without winding has MAX/MIN temperature of 386K/372K as shown in the inset of Fig. 5(c). The model shows that the inner loop is hotter than the outer loop during the period from 0 to 10^4 seconds due to the higher peak flux density that is expected for a toroidal core geometry. Additional hot spots tend to be observed at the location of the windings where the convection is restricted causing heat accumulation. The model reproduces the tendency to form a higher temperature region at the inner core radius that agrees well with the infrared thermal imaging results as shown in Fig. 4. Figure 5(c) shows the volume-averaged temperature changes as a function of heating time. Since power transformers and many distribution transformers are oil immersed, an accurate prediction of core temperature becomes more difficult to achieve unless a more sophisticated heat transfer model is created by the finite element method.

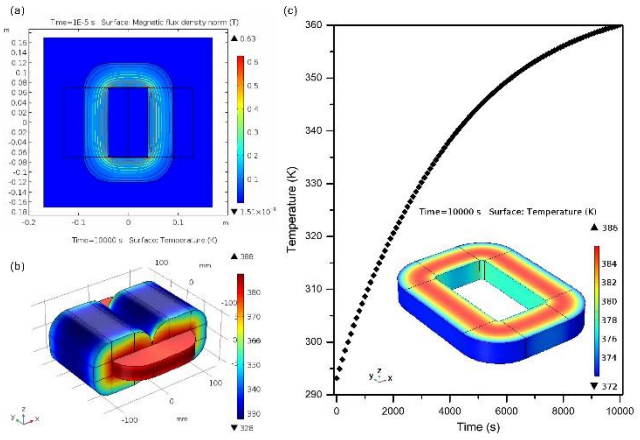

Fig. 5. (a) Magnetic flux density normal distribution and contour plot of the magnetic vector potential in the core at t = 0.01ms. (b) FEM simulation results of temperature distribution of the core including windings at $t = 10^4$s. (c) The volume-averaged temperature changes as a function of heating time. Inset shows temperature distribution of the core without windings at $t = 10^4$s.

Validation experiments are conducted to verify the finite element analysis results, by comparing the data measured by the conventional infrared thermal imaging inspection method and the proposed fiber optic temperature sensor. While the model can approximately simulate the heat dissipation process in the transformer, discrepancies between the real performance and the simulation are likely due to limitations of this simplified model which does not consider the actual heat conduction, convection, and radiation in the complex test environment so as to simplify calculations. The peak temperature rise at the location of the winding can't be clearly resolved with the infrared thermal imaging results due to a lack of optical access to the core in that region. While the OFDR-based distributed fiber sensor is capable of creating a 3D map of heat distribution and thus it is more appropriate to validate the temperature model by measuring temperature rise online. A reference optical time-domain-like trace is shown in Fig. 6. Therein, the FC/APC connector at the front panel of the OFDR is visible along with the fusion splicing point and the Rayleigh backscattering along the length of the fiber. It is noted that ~1.5 dB loss is caused by the sharp bend of the sensing fiber at the corners of the inner loop and no extra loss is found at the outer loop corner position because of a much larger fiber bend radius over 2 cm. Other Rayleigh spectra are obtained when the transformer is in operation with the conditions described above.

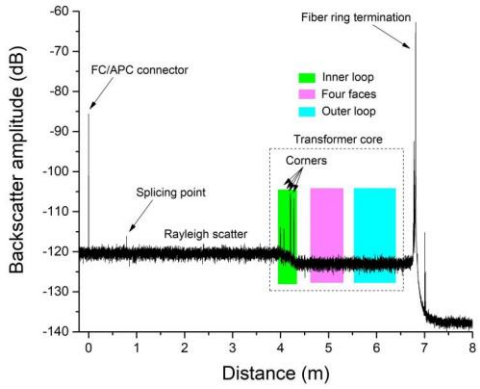

Fig. 6. Reference backscatter signals versus distance along the sensing fiber instrumented on the transformer core.

Figure 7 shows the temperature change profile along the sensing fiber at 60 minutes of heating from the transformer core. The inner loop shows a higher temperature compared to the outer loop which agrees well with both the thermal camera results and FEM simulation results. It is obvious that this system provides measurement-information from areas which are not accessible by the thermal camera such as the insulation barrier/winding covered area, the back of the core, and the area blocked by the metal frame. The ability to measure local temperatures in excited transformer cores in regions which do not provide optical access for standard IR-based imaging methodologies is a significant advantage of the fiber-based temperature monitoring approach demonstrated in this work.

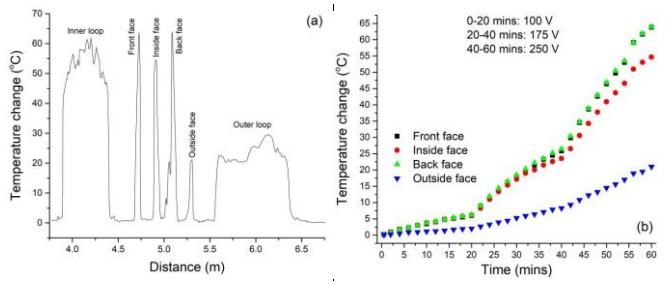

Fig. 7. (a) The heating profiles at 60 minutes. (b) Temperature changes as a function of heating time at various locations on the transformer core.

B. MANC-type Core

After evaluating the FT-3TL core, the MANC-type core is measured in a similar fashion. A reference optical time-domain-like trace at room temperature is shown in Fig. 8. Rayleigh spectra are continuously recorded when the transformer is in operation with an input voltage amplitude of 100V.

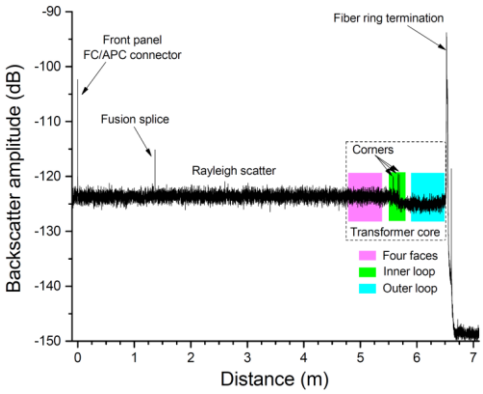

Fig. 8. Reference backscatter signals versus distance along the sensing fiber instrumented on the transformer core.

The maximum error in the spectral shift induced by performing cross-correlation between the reference and measurement spectra in a given gauge length determines the temperature accuracy. It is obvious that the increased gauge length will reduce the uncertainty of the spectral shift at the cost of the reduced spatial resolution. The spectral shift quality Q is used to characterize the degree of correlation between reference and measurement spectra defined by $Q = \max[C(S_R, S_R)]/\max[C(S_R, S_M)]$, where $\max[C(S_R, S_R)]$ is the maximum value of the reference spectra auto-correlation, and $\max[C(S_R, S_M)]$ is the maximum of the cross-correlation of the reference and measurement spectra. The spectral shift quality Q is simulated under different OFDR configurations. It is indicated that Q could decrease from ~0.9 to ~0.1 as the gauge length is decreased by a factor of 10, showing an inherent trade-off between the sensing accuracy and spatial resolution under a fixed level of perturbation. Furthermore, the temperature fluctuation is only ~ 0.1°C for Q = 0.85 while the standard deviation in the temperature measurement is as high as ~ 10°C as Q drops to 0.15. Large temperature variations and other factors like vibration, optical fiber being stretched or bent, and adoption of multimode sensing fiber can affect the Q-value as well as the sensor accuracy. Thus, the sensing accuracy is directly related to the spectral shift quality. When the gauge

length is selected to be 1 cm, the temperature accuracy is ~0.1°C for typical OFDR applications where Q is larger than 0.85. The highest long-term reliability among polymer coatings of optical fibers is inherent to the coatings based on acrylate or polyimides, which allows the use of fiber sensors in high temperature power transformer by maintaining high Q-values.

Figure 9 shows the spectral shift between the reference and measurement cross-correlated Rayleigh spectra along the sensing fiber after 2 minutes of heating from the transformer core. In general, the data sets are considered well correlated as Q is approaching 1.0. The spectral shift quality is evaluated by setting two thresholds at Q = 0.85 and Q = 0.15, corresponding to temperature accuracy of ~0.1°C and ~10°C respectively. In the first region above the ($0.85<Q<1.0$) threshold, the spectral shift data is considered effective and reliable. The region between two thresholds ($0.15<Q<0.85$) indicates less reliable spectral shift data. This could be for instance due to the thermal stress is induced onto the sensing fiber; particularly at the inner loop corners where the optical fiber is sharply bent. This has the effect of reducing the temperature accuracy to about 1 degree Celsius as Q = 0.5. The third region defined as $0<Q<0.15$ leads to invalid spectral shift values that indicate unreliable temperature measurement data. To improve the temperature accuracy at those corner regions, a longer data segment or larger correlation window can be used to prevent distortion in the position scale, but sacrifices some spatial resolution. In temperature sensing experiments, measurement accuracy deteriorates as the fiber length or measurement range extends because: 1) phase noise of the tunable laser source leads to a reduced coherent length; 2) errors in the resampled beat signal accumulate at the far end of the sensing fiber and result in worse spatial resolution; 3) increased phase noise at a longer distance disturb the local Rayleigh backscattering profile and causes imprecise spectral shift values and temperature readings. Considering the above factors, the proposed OFDR-based fiber sensor can achieve 1cm spatial resolution with a total length up to 70 m, meeting dimension requirements in typical large power transformers. The localized temperature measurement accuracy within a certain spatial region ranges from 0.1°C to a few degree Celsius depending on the actual operation conditions. It is also noted that unreliable spectral shift data at any specific location would not affect the validity of other sensing data since Q is not a cumulative value on the fiber distance.

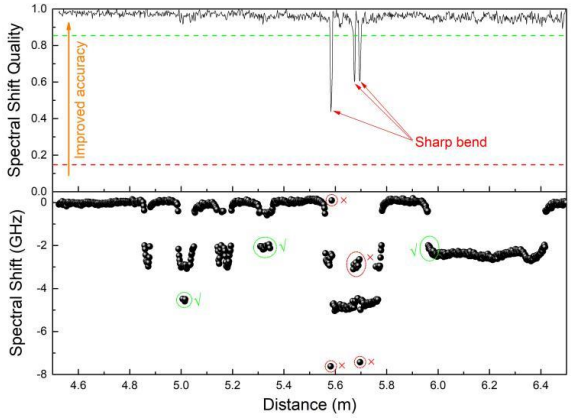

Fig. 9. (Top) Spectral shift quality analysis result; (Bottom) Distributed spectral shift at 2 minutes.

Next, some transient measurements were made on the core under test to illustrate the utility of the system in collecting relevant transient information. The red curve in Fig. 10 is the reference heating profile along the sensing fiber before temperature tests. The blue and black curves in Fig. 10 represent the heating profiles along the sensing fiber after 0 and 2 minutes of heating from the core. Temperature variations as small as 0.1°C can be clearly observed and resolved at these early stages of the magnetic core heating process while still not approaching the thermal steady state. In this case, the time required for OFDR measurement is 2 seconds to complete laser wavelength scanning, data acquisition and processing. This value represents the time-resolution capable in this measurement example which could be improved by operating the TLS at a faster wavelength tuning speed or using a higher speed data acquisition device.

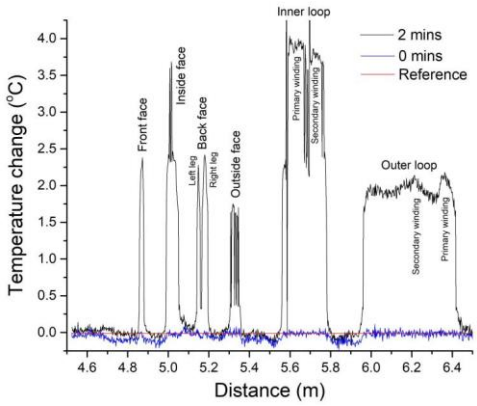

Fig. 10. The reference heating profile along the sensing fiber (red); the heating profiles at 0 (black) and 2 (blue) minutes of heating from the transformer core.

In some cases of more intense heating coupled with small fiber-bend radii, more positions along the sensing fiber fall within the ($0.15<Q<0.85$) region where the temperature accuracy is greatly reduced. The spectral shift data are still considered to be valid, but with reduced temperature accuracy reflecting additional thermal stress effects. We then define the term "equivalent temperature changes" as temperature changes calculated from the overall spectral shift. Spectral shift and quality analogous of this measurement situation are shown in Figure 11. Figure 12 shows the heating profiles along the same sensing fiber, which has been heated for 28 minutes to produce this condition. It is noted that the regions around the primary and secondary windings in both the inner loop and outer loop have relatively high equivalent temperature changes based upon the observed spectral shifts. Those locations are where the insulation paper is inserted between the core and windings surrounding the sensing fiber, restricting air flow and creating hot spots. Direct mechanical contact between the windings and core surface and optical fiber can also increase the sensitivity to thermally generate stresses on the fiber in this region as well, which will be convoluted with pure temperature effects.

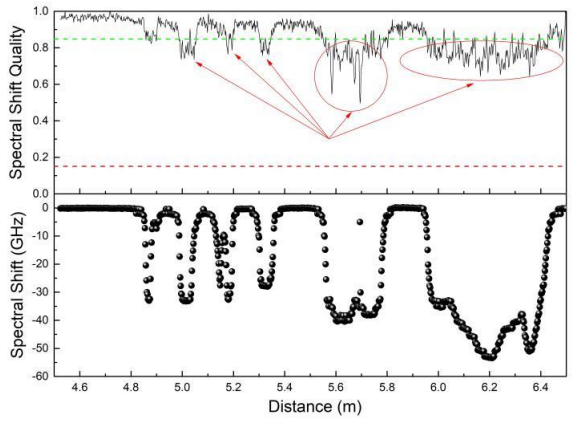

Fig. 11. (Top) Spectral shift quality analysis result. (Bottom) Spectral shift of cross-correlation calculation between the reference and test Rayleigh spectra along the sensing fiber at 28 minutes of heating from the transformer core.

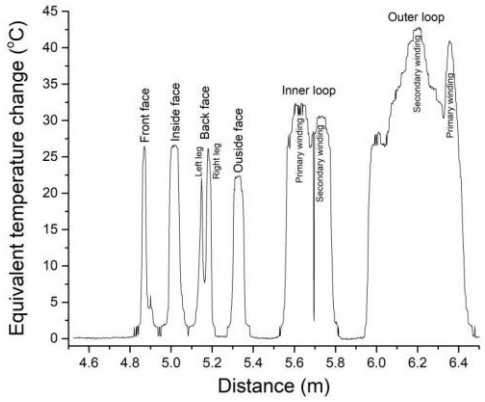

Fig. 12. The heating profile at 28 minutes.

The LUNA-OBR is capable of performing a complete measurement in a few seconds. Monitoring of the monotonous temperature rise of the transformer can thus be realized in real time during a 30-minute test period with as many as hundreds of resolved-data points. Figure 13 shows the heating profiles along the sensing fiber at 10, 20, and 30 minutes of heating from the transformer core. It shows that the inner loop/inside face is hotter than the outer loop/outside face at the beginning of the temperature rising period. Then, the outer loop spectral shift increases much faster than the inner loop because of different levels of thermal stress despite the fact that the inside face remains hotter than the outside face in terms of actual temperature measurements. The infrared thermal camera measures the temperature rise of the transformer as shown in the inset of Fig. 13. The temperature on the maximum and minimum scales are 41.9ºC and 22.6ºC, corresponding to the locations of observable region of the inner loop and ambient air. Their temperature difference is about 20ºC, which agrees well with that measured by using the fiber optic sensor method.

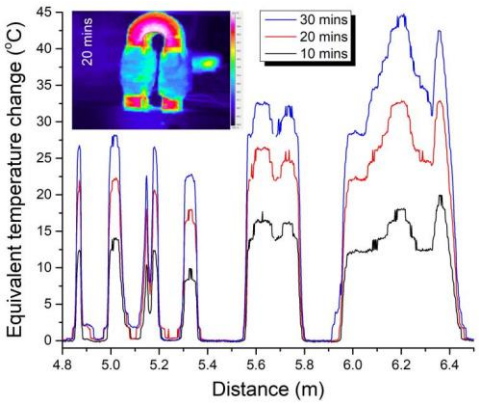

Fig. 13. The heating profile of the sensing fiber at 10, 20, and 30 minutes. Inset is the infrared thermal image recorded at 20 minutes.

A linear regression analysis was performed on the time-history data to illustrate the time-dependence of the heating profiles, as shown in Fig. 14. It demonstrates that the winding regions have the fastest rise in temperature for a 30-minute period before the steady state is reached. This occurs because the insulation barrier regions surrounding the core form a non-exposed area where the windings generate non-negligible heat, leading to an enhanced temperature gradient near those regions. As expected, the measured temperatures throughout the core are highly dependent on the core geometry and thermal conduction paths for the core with which it was instrumented. For well-designed transformers, the temperature eventually approaches a steady state value, which varies spatially throughout the core and depends upon the details of thermal management, excitation conditions, and core geometry among other factors. Continuous on-line temperature rise monitoring can also be used to predict maximum temperatures at thermal equilibrium by fitting the time-history data to an exponential curve. The time dependent temperature changes can be expressed as $\Delta T(t)=\Delta T_0 \exp(t/\tau)$, where ΔT_0 is the initial temperature difference at t = 0, and τ is the characteristic thermal time constant. As shown in Fig. 14, extrapolation with exponential curve fitting predicts the steady-state working temperature. For instance, the primary and secondary windings in the outer loop would show a temperature rise of ~93°C and ~62°C respectively above a 20°C ambient temperature provided that the core heats continuously for 3 hours. By inspecting the thermal trending during early stages of excitation for prototype designs via this real-time fiber optic sensing method, prototype failures can be prevented well before they occur. The sensing fiber (SMF28, Corning) used in this study operates continuously at 85ºC with occasional excursions to 100ºC. To achieve long-term high reliability of the fiber temperature sensor for typical power transformers designed for a maximum temperature rise up to 150-200ºC, it is necessary to adopt polyimide coated fibers which can withstand continuous temperatures of 300°C and short-term temperatures as high as 400°C.

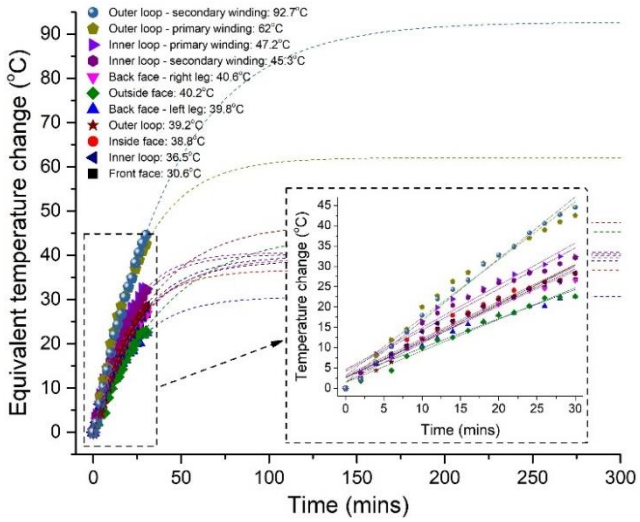

Fig. 14. Temperature changes as a function of heating time at various locations on the transformer core. Inset is the continuous on-line sensing of temperature rise predicts thermal equilibrium by data fitting.

One of the ultimate goals of the unique testing facilities established and described in this effort is the ability to locally measure and quantify core heating and steady state operational conditions. It can develop a quantitative understanding of the relationship with core fabrication/processing methodologies. It can also help to optimize the detailed excitation conditions to which the transformer core is subjected and quantify the associated core and winding losses. In the short term, this unique capability will provide transformer designers with new information that was previously inaccessible to assist in the design and realization of transformers with controlled temperature rise as required for a particular application. In the future, similar methodologies can also be adapted for the purpose of real-time asset monitoring of power transformers deployed in the field to provide early indications of potential failure to enable preventative maintenance [45], [46]. Barring fiber damage, the sensing fibers are engineered with a minimum design life of 25 years. The limiting factor of the realistic lifespan is the long term stress on the fiber operating above the design temperature.

IV. Conclusion

We have proposed and experimentally demonstrated OFDR-based fiber sensors for distributed real-time temperature monitoring in operating power transformers. The dimensions of a compact medium frequency transformer design create a challenge for conventional sensing methods to access. The small size and high flexibility of optical fibers make it possible to install the sensing fiber in a distributed fashion over the core structure without affecting temperature measurement precision. In addition, the dynamic temperature rising process can be effectively monitored by the optical fiber sensor in locations where it is difficult to perform continuous thermal imaging. Thus, regions of the core not exposed to optical access can be investigated. While initial measurements were successful, some of the finer details of this type of measurement are still undiscovered. In particular, the effects of combined thermal-stress will be further explored, and other techniques for eliminating cross-sensitivity between temperature rise and thermally induced strains will be examined. All the fiber optic sensors including both distributed and single-point ones are limited by the inherent temperature-strain cross-sensitivity effects. Although discrete point-wise temperature sensors have more flexible structures to be tailored with strain insensitive properties. Nevertheless, the results here clearly demonstrate that the fiber-optic sensor provides an effective solution to monitoring the physical transformer core structure as well as accurately detecting the non-uniform temperature distribution inside the wound transformer. The sensor system can provide informative feedback to the transformer designer. In the longer term, such approaches may open the door for novel approaches to real-time asset monitoring of power transformers while in operation. The spatial resolution of this sensing method will also be useful in future designs of magnetic cores where heterogeneous strain annealing profiles or other advanced manufacturing techniques are used for targeted thermal management.

V. References

[1] R. Godina, E.M.G. Rodrigues, J.C.O. Matias, and J.P.S. Catalão, "Effect of loads and other key factors on oil-transformer ageing: sustainability benefits and challenges," Energies, vol. 8, no. 10, pp. 12147-12186, 2015.

[2] H. Hamzehbahmani, A. J. Moses and F. J. Anayi, "Opportunities and precautions in measurement of power loss in electrical steel laminations using the initial rate of rise of temperature method," IEEE Trans. Magn., vol. 49, no. 3, pp. 1264-1273, 2013.

[3] W.J. McNutt, J.C.McIver, G.E. Leibinger, D.J. Fallon, K.A. Wickersheim, "Direct measurement of transformer winding hot spot temperature" IEEE Trans. Power Apparatus and Systems, vol. 103, no. 6, pp. 1155-1162, 1984.

[4] T.D. Poyser, D.A. Yannucci, J.B. Templeton, B.N. Lenderking, "On-line monitoring of power transformers," IEEE Trans. Power Apparatus and Systems, vol. 104, no. 1, pp. 207-211, 1985.

[5] C. Sun, P.R. Ohodnicki, and M. S. Emma, "Chemical sensing strategies for dissolved gas analysis in transformer oil: A review," IEEE Sens. J., vol. 17, no. 18, pp. 5786-5806, 2017.

[6] P.R. Ohodnicki, J. Baltrus, and T. Brown, "Pd/SiO_2 and AuPd/SiO_2 nanocomposite-based optical fiber sensors for H_2 sensing applications," Sens. Actuators B Chem., vol. 214, pp. 159-168, 2015.

[7] M. Wang, A. Vandermaar, and K.D. Srivastava, "Review of condition assessment of power transformers in service," IEEE Electr. Insul. Mag., vol. 18, no. 6, pp. 12-25, 2002.

[8] A.M. Leary, P.R. Ohodnicki, and M.E. McHenry, "Soft magnetic materials in high-frequency, high-power conversion applications," The Journal of The Minerals, Metals & Materials Society (TMS), vol. 64, no. 7, pp. 772-781, 2012.

[9] P.R. Ohodnicki, A.M. Leary, M.E. McHenry, F. Filho, G. Nojima, and A. Hefner, "State-of-the-art of HF soft magnetics and HV/UHV silicon carbide semiconductors," PCIM Europe 2016; International Exhibition and Conference for Power Electronics, Intelligent Motion, Renewable Energy and Energy Management, Nuremberg, Germany, 2016, pp. 1-10.

[10] S.A. Ryder and I.J. Vaughan, "A simple method for calculating core temperature rise in power transformers," IEEE Trans. Power Del., vol. 19, no. 2, pp. 637-642, 2004.

[11] S. Purushothaman and F. de León, "Heat-transfer model for toroidal transformers," IEEE Trans. Power Del, vol. 27, no. 2, pp. 813-820, 2012.

[12] A.A. Boiarski, G. Pilate, T. Fink, "Temperature measurements in power plant equipment using distributed fiber optic sensing," IEEE Trans. Power Del., vol. 10, no. 4, pp. 1771-1778, 1995.

[13] H. Nordman and M. Lahtinen, "Thermal overload tests on a 400-MVA power transformer with a special 2.5-p.u. short time loading capability," IEEE Trans. Power Del., vol. 18, no. 1, pp. 107-112, 2003.

[14] T.K. Gangopadhyay, C.P. Mukul, and L. Bjerkan, "Fiber-optic sensor for real-time monitoring of temperature on high voltage (400KV) power transmission lines," Proc. SPIE, vol. 7503, pp. 75034M, 2009.

[15] D.J. Kweon, K.S. Koo, J.W. Woo, and J.S. Kwak, "A study on the hot spot temperature in 154kV power transformers," J. Electr. Eng. Technol., vol. 7, no. 3, pp. 312-319, 2012.

[16] P. Lu, K. Byerly, M. Buric, P. Zandhuis, C. Sun, A. Leary, R. Beddingfield, M.E. McHenry, and P.R. Ohodnicki, "Distributed fiber-optic sensor for real-time monitoring of energized transformer cores", Proc. SPIE, vol. 10194, pp. 101941S, 2017.

[17] C. Sun, P. Lu, R. Wright, and P.R. Ohodnicki, "Low-cost fiber optic sensor array for simultaneous detection of hydrogen and temperature," Proc. SPIE, vol. 10654, pp. 1065405, 2018.

[18] A. Yan, S. Li, Z. Peng, R. Zou, P. Ohodnicki, P. Lu, K. Byerly, M.J. Li, and K.P. Chen, "Multi-point fiber optic sensors for real-time monitoring of the temperature distribution on transformer cores," Proc. SPIE, vol. 10639, pp. 1063912, 2018.

[19] P. Duwez, R. H. Willens, and W. Klement, “Continuous series of metastable solid solutions in silver-copper alloys,” J. Appl. Phys., vol. 31, no. 6, pp. 1136-37, 1960.

[20] P. Duwez and S.C.H. Lin, “Amorphous ferromagnetic phase in iron-carbon-phosphorus alloys,” J. Appl. Phys., vol. 38, no. 10, pp. 4096-4097, 1967.

[21] R. Hasegawa, “Amorphous magnetic materials, a history,” J. Mag. Mag. Mat., vol. 100, no. 1-3, pp. 1-12, 1991.

[22] H.S. Chen and D.E. Polk, “Novel amorphous metals and amorphous metal articles,” U.S. Patent No. 3856513 (1974).

[23] R. Hasegawa, R.C. O'Handley, L.E. Tanner, R. Ray and S. Kavesh, “Magnetization, magnetic anisotropy, and domain patterns of $Fe_{80}B_{20}$ glass,” Appl. Phys. Lett., vol. 29, no. 3, pp. 219-211, 1976.

[24] R.C. O'Handley, C.P. Chou and N. DeCristofaro, “High-induction low-loss metallic glasses,” J. Appl. Phys. 50, 3603, (1979).

[25] N. DeCristofaro, A. Datta, L.A. Davis and R. Hasegawa, Proc. 4th Intern. Conf. Rapidly Quenched Metals, eds. T. Masumoto and K. Suzuki (The Japan Inst. Metal, 1031, 1982).

[26] N. DeCristofaro, A. Freilich and D. Nathasingh, “Iron-metalloid amorphous alloys for electromagnetic devices,” U.S. Patent No. 4219355, 1980.

[27] M. Mitera, T. Masumoto and N.S. Kazama, “Effect of silicon addition on the magnetic properties of Fe-B-C amorphous alloys,” J. Appl. Phys., vol. 50, no. B11, pp. 7609-7611, 1979.

[28] F.E. Luborsky and J. Walter, “Preparation and properties of Fe-B-Si-C amorphous alloys,” IEEE Trans. Mag., vol. 16, no. 4, pp. 572-574, 1980.

[29] Y. Yoshizawa, S. Oguma and K. Yamauchi, “New Fe-based soft magnetic alloys composed of ultrafine grain structure,” J. Appl. Phys., vol. 64, no. 10, pp. 6044-6046, 1988.

[30] M.E. McHenry, M.A. Willard, and D.E. Laughlin, “Amorphous and nanocrystalline materials for applications as soft magnets,” Prog. Mat. Sci., vol. 44, no. 4, pp. 291-433, 1999.

[31] A. Leary, V. Keylin, A. Devaraj, V. DeGeorge, P. Ohodnicki and M.E. McHenry, “Stress induced anisotropy in co-rich magnetic nanocomposites for inductive applications.” J. Mat. Res., vol. 31, no. 20, pp. 3089-3107, 2016.

[32] M. E. McHenry and D. E. Laughlin; Chapter 19 - Magnetic properties of metals and alloys. Physical Metallurgy - 5th Ed., Elsevier B.V. pp. 1881-2008, 2015.

[33] M.E. Froggatt, D.K. Gifford, S.Kreger, M. Wolfe, and B.J. Soller, “Characterization of polarization-maintaining fiber using high-sensitivity optical-frequency-domain reflectometry,” J. Light. Technol., vol. 24, no. 11, pp. 4149-4154, 2006.

[34] M. Froggatt, and J. Moore, "High resolution strain measurement in optical fiber with Rayleigh scatter," Appl. Opt., vol. 37, no. 10, pp. 1735-1740, 1998.

[35] B.J. Soller, D.K. Gifford, M.S. Wolfe, and M.E. Froggatt, "High resolution optical frequency domain reflectometry for characterization of components and assemblies," Opt. Express, vol. 13, no. 2, pp. 666-674, 2005.

[36] M. Buric, P. Ohodnicki, A. Yan, S. Huang, and K.P. Chen, "Distributed fiber-optic sensing in a high-temperature solid-oxide fuel cell," Proc. SPIE, vol. 9977, no. 997708, 2016.

[37] J. Song, W. Li, P. Lu, Y. Xu, L. Chen, and X. Bao, "Long-range high spatial resolution distributed temperature and strain sensing based on optical frequency-domain reflectometry", IEEE Photon. J., vol. 6, no. 3, pp. 1-8, 2014.

[38] M. Ren, P. Lu, L. Chen, and X. Bao, "Theoretical and experimental analysis of Φ-OTDR based on polarization diversity detection," IEEE Photonc. Tech. L., vol. 28, no. 6, pp. 697-700, 2016.

[39] P. Lu and Q. Chen, "Optical low-coherence reflectometry for deflection measurement with a fiber Bragg grating cantilever sensor", Meas. Sci. Technol., vol. 20, no. 7, pp. 075303, 2009.

[40] https://www.hitachi-metals.co.jp/products/elec/tel/pdf/hl-fm30-b.pdf

[41] S. Simizu, P.R. Ohodnicki, and M.E. McHenry, "Metal amorphous nanocomposite soft magnetic material-enabled high power density, rare earth free rotational machines," IEEE Trans. Mag., vol. 54, no. 5, pp. 8202505, 2018.

[42] J. Muhlethaler, J. Biela, J. W. Kolar and A. Ecklebe, "Core losses under the DC Bias condition based on Steinmetz parameters," IEEE Trans. Power Electr., vol. 27, no. 2, pp. 953-963, 2012.

[43] R. Gong, J. Ruan, J. Chen, Y. Quan, J. Wang, and C. Duan, "Analysis and experiment of hot-spot temperature rise of 110 kV three-phase three-limb transformer," Energies, vol. 10, no. 8, pp. 1079 (2017).

[44] Mst. Nazmunnahar, S. Simizu, P.R. Ohodnicki, S. Bhattacharya, and M.E. McHenry, “Finite element analysis modeling of high voltage and frequency 3-phase solid state transformers enabled by metal amorphous nanocomposites,” J. Mater. Res., vol. 33, no. 15, pp. 2138-2147, 2018.

[45] K. Byerly, R. Ohodnicki, S.R. Moon, A.M. Leary, V. Keylin, M.E. McHenry, S. Simizu, R. Beddingfield, Y. Yu, G. Feichter, R. Noebe, R. Bowman, and S. Bhattacharya, “Metal amorphous nanocomposite (MANC) alloy cores with spatially tuned permeability for advanced power magnetics applications,” J. Mater., vol. 70, no. 6, pp. 879-891, 2018.

[46] R. Beddingfield, K. Byerly, S. Simizu, A. Leary, S. Bhattacharya, P. Ohodnicki, and M.E. McHenry, “Thermal profile shaping and loss impacts of strain annealing on magnetic ribbon cores,” J. Mater. Res., vol. 33, no. 15, pp. 2189-2206, 2018.